ICAS 2021 SHANG HAI
32nd Congress of the International Council of the Aeronautical Sciences
September 6-10, 2021 Pudong Shangri-La, Shanghai, China

STUDY OF SMALL UAVS DISTURBED MOTION NATURAL FREQUENCIES USING EXTENDED EXPERIMENTAL DATASETS

Mostafa El-Salamony[1] & Sergey Serokhvostov [4]

[1] Peking University, Beijing, China
elsalamony.mostafa@pku.edu.cn

[2] Moscow Institute of Physics and Technology, Dolgoprudny, Russia
serokhvostov@phystech.edu

Abstract

This article aims to study the disturbed motion natural frequencies of small Unmanned Aerial Vehicles (UAVs) of glider type and evaluate the available analytical methods based on extended experimental results obtained from different measuring devices and at different velocities for two aircraft. This article completes and overcomes the deficiencies of the previous analyses.

Keywords: Stability; Natural Frequency; Long Mode; Short Mode; Autopilot.

1. Introduction

Since the UAVs are designed according to the procedure used for the large aircraft, the stability calculations usually also follow the same formulae derived for the large aircraft. However, the length scale of small UAVs is much smaller. Hence, the aerodynamic forces and loads, which are applied on the UAV, inertia momentums and others change their magnitude nonlinearly and not proportionally to each other with length scaling. Consequently, some assumptions for the large aircraft are violated in such case, and new assumptions can be introduced which are only valid for the small ones. Attempts of preliminary investigations were conducted previously to evaluate the accuracy of using the analytical / empirical formulas of natural frequencies. Formulas of Roskam [[1]], Hull [[2]] and Ostoslavsky [[3]] are investigated.

The longitudinal flight modes (short and long modes) were investigated in detail in [[4], [5]], and the Dutch roll oscillation of the lateral motion was investigated in more detail [[6]]. This research considered the natural frequencies of longitudinal and lateral motions calculated by the conventional methods of estimation for the manned aircraft provided in literature, and the numerical VLM program XFLR5 with experimental values of real flight. A special procedure of comparing theoretical and experimental results was proposed for the case of small UAVs. Some preliminary results of these investigations are as follows. The assumption of separating the disturbed aircraft motion to longitudinal and lateral motions is valid for small UAVs. Separation of longitudinal disturbed motion to long and short modes is possible for at least the UAVs having conventional configuration since the short mode frequency is at least several times higher than the one of the long mode. For the long mode, the approximate methods of Roskam and Hull are not correct in case of small UAVs. Considering the short mode, all methods can predict the frequency with good accuracy.

As for the Dutch roll natural frequency [6], the approximate method of Roskam underestimates the frequency and hence the assumptions used are not valid in case of small UAVs.

Fuselage contribution in the natural frequencies is investigated by means of analytic and numerical methods and validated by means of experimental data [[7]]. It is found that for slender fuselage, its contribution in aerodynamic and stability derivatives is negligible. By neglecting the fuselage, the short and long mode frequencies slightly decrease, and the Dutch roll frequency slightly increases. The numerical method shows that fuselage contributes strongly in damping ratios. Neglecting the fuselage leads to reduction in short mode damping ratio and increases the damping ratios of long and Dutch roll

modes. Analytic and numerical methods show the same qualitative results, which increases the confidence in the results. The results are compared with experimental results and showed good convergence, which support the proposal that neglecting the fuselage will not affect the natural frequencies for small UAVs.

The main shortages in the previous studies can be summarized as follows. The tests are conducted at one speed. Hence, the degree of certainty in matching the experimental and calculated frequencies is questionable. Besides, the device used in measuring the flight angles has sampling rate close to the frequency of the short mode. So, the possibility of aliasing or frequency smearing is big. In addition, the dataset used is limited to few flights with short time span of steady free flight.

In this article, the shortages of the previous studies are considered. The analysis is done for two different UAVs, Sonic 185 [[8]] and Cirrus [[9]]. The range of flight velocities is extended from 5 to 12 m/s. Different measuring devices are used, namely AuduPilot, SmartAP, and PixHawk, which have different sampling frequencies.

This article is organised as follows. The UAVs are introduced in Section 2, followed by reviewing the analytical approach, based on Roskam approach, in Section 3. The experimental setup and data analysis are discussed in Section 4, followed by the conclusion in Section 5.

2. Studied Aircraft Models

Two different UAV configurations were included in this study. Sonic 185 of DYNAM [[8]] is a conventional glider UAV with design cruise speed 10 m/s and wing span 1.85 m. Cirrus glider of Reichard Modelsport [[9]] has design cruise velocity 6 m/s, wing span of 3.4 m and small dihederal angle near the wing tips. Data of these models are stated in Tables 1-3, and their geometries are shown in Figures 1 and 2.

Table 1 Aircraft parameters

Property	**Sonic 185**	**Cirrus**
Mass [kg]	1.18	1.97
Span [m]	1.85	3.4
Wing area (S) [m^2]	0.33	0.698
Cruise velocity [m/s]	8	6
Moments of Inertia:		
Ixx [kg·m^2]	0.108	0.979
Iyy [kg·m^2]	0.065	0.149
Izz [kg·m^2]	0.122	0.753
Airfoil	E231	NH F3J
CG from leading edge of root section [m]	0.07	0.11

Table 2 Aircraft Sonic 185 geometry

Property	**Wing**	**Hor. Tail**	**Ver. Tail**
Aspect ratio	10.295	4.92	2.03
Mean chord [m]	0.189	0.1	0.16

Span [m]	1.85	0.48	0.16
Root chord [m]	0.205	0.125	0.2
Tip chord [m]	0.06	0.02	0.115
Sweep angle from leading edge [deg]	6.71	18.17	23.25

Table 3 Aircraft Cirrus geometry

Property	**Wing**	**Hor. Tail**	**Ver. Tail**
Aspect ratio	16.556	6.03	4
Mean chord [m]	0.216	0.1	0.11
Span [m]	3.4	0.3	0.21
Root chord [m]	0.245	0.115	0.15
Tip chord [m]	0.06	0.06	0.05
Sweep angle from leading edge [deg]	4.67	23.57	7.83

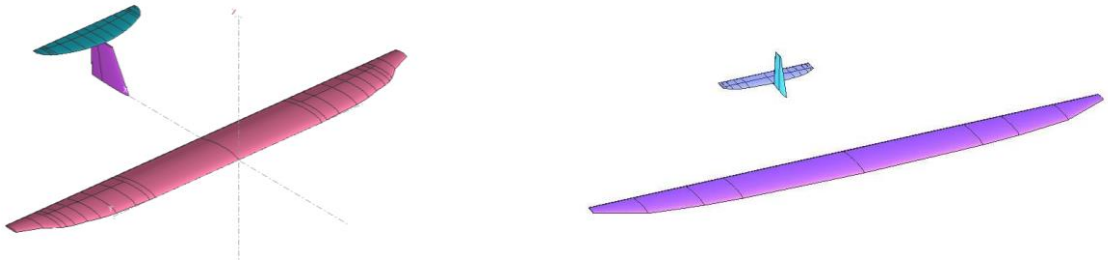

Figure 1 Sonic 185 and Cirrus UAVs, plotted in XFLR5

The aerodynamic and stability coefficients are calculated according to Roskam [8] and the results are presented in Tables 4 and 5 for Sonic 185 for longitudinal and lateral directions respectively. As for Cirrus, the derivatives are presented in Tables 6 and 7. It shall be noticed that Cmq in the equations used in Roskam procedure is twice the one in Ostoslavsky procedure by definition [[5]].

Table 4 Aerodynamic longitudinal derivatives of Sonic 185

Derivative	**Angle of attack (α)**	**Pitch rate (q)**	**Rate change of angle of attack (α˙)**
Lift coefficient (CL)	5.253	7.312	4.655
Drag coefficient (CD)	0.377	0	0
Moment coefficient (Cm)	-0.47	-8.59	-5.1337

Table 5 Aerodynamic lateral derivatives of Sonic 185

Derivative	**Sideslip Angle (β)**	**Roll Rate (p)**	**Yaw Rate (r)**
Side Force Coeff. (Cy)	−0.17	0	0.14
Roll Moment Coeff. (Cl)	−0.113	−0.873	0.204
Yaw Moment Coeff. (Cn)	0.064	−0.127	0.124

Table 6 Aerodynamic longitudinal derivatives of Cirrus

Derivative	**Angle of attack (α)**	**Pitch rate (q)**	**Rate change of angle of attack (α˙)**
Lift coefficient (CL)	5.841	7.92	4.468
Drag coefficient (CD)	0.532	0	0

Moment coefficient (Cm)	-0.743	-17.584	-5.245

Table 7 Aerodynamic lateral derivatives of Cirrus

Derivative	Sideslip Angle (β)	Roll Rate (p)	Yaw Rate (r)
Side Force Coeff. (Cy)	−0.2236	0	0.115
Roll Moment Coeff. (Cl)	−0.3216	−1.415	0.3353
Yaw Moment Coeff. (Cn)	0.0584	−0.6437	0.2115

3. Overview on the Analytical Procedure

3.1 Roskam Method

In this section the procedures of Roskam (exact and approximate) are considered together due to the fact that they have quite similar equations and results as a sequence.

The characteristic equation of Roskam [[1]] is

$$ax^4 + bx^3 + cx^2 + dx + e = 0 \tag{1}$$

where

$$a = U_1 - Z_{\dot{\alpha}} \tag{2}$$

$$b = -(U_1 - Z_{\dot{\alpha}})(X_u + X_{Tu} + M_q) - Z_\alpha - M_{\dot{\alpha}}(U_1 - Z_q) \tag{3}$$

$$c = (X_u + X_{Tu})\left[M_q(U_1 - Z_{\dot{\alpha}}) + Z_\alpha + M_{\dot{\alpha}}\left(U_1 + Z_q\right)\right] + M_q Z_\alpha - Z_u X_\alpha + M_{\dot{\alpha}} g \sin\theta_1 - \left(M_\alpha + M_{T_\alpha}\right)\left(U_1 + Z_q\right) \tag{4}$$

$$d = g\sin\theta_1\left[M_\alpha + M_{T_\alpha} - \left(M_{\dot{\alpha}} * \left(X_u + X_{T_u}\right)\right] + g\cos\theta_1\left[Z_u * M_{\dot{\alpha}} + \left(Mu + M_{T_u}\right) * (U_1 - Z_{\dot{\alpha}})\right] + \left(M_u + M_{T_u}\right) * \left[-X_\alpha(U_1 + Zq)\right] + Z_u X_\alpha M_q + \left(X_u + X_{T_u}\right)\left[\left(M_\alpha + M_{T_\alpha}\right)(U_1 + Z_q) - M_q Z_\alpha\right] \tag{5}$$

$$e = g\cos\theta_1\left[Z_u\left(M_\alpha + M_{T_\alpha}\right) - Z_\alpha\left(M_u + M_{T_u}\right)\right] + g\sin\theta_1\left[X_\alpha\left(M_u + M_{T_u}\right) - \left(X_u + X_{T_u}\right)\left(M_\alpha + M_{T_\alpha}\right)\right] \tag{6}$$

After replacing these coefficients, one will have a fourth order equation that describes the two modes. To simplify the analysis, one can assume that the time scale of both modes is much different. Hence, the approximate solution for the natural frequency of the short and long modes eventually becomes:

$$\omega_{n,short\ period} = \sqrt{\frac{Z_\alpha * M_q}{U_1} - M_\alpha} \tag{7}$$

$$\omega_{n,long\ period} = \sqrt{\frac{-Z_u * g}{U_1}} \tag{8}$$

3.2 Ostoslavsky Procedure

Ostoslavsky method [[3]] is good method for direct determination of what parameters affect the frequencies. He introduced the characteristic equation of the system as fourth order function in its eigen values as:

$$F = \lambda^4 + a_1\lambda^3 + a_2\lambda^2 + a_3\lambda^2 + a_4\lambda = 0 \tag{11}$$

where the coefficients of this equations under the steady state condition are:

$$a_1 = C_{L\alpha} - \frac{C_{m_{\dot{\alpha}}} + C_{m_q}}{\bar{r_z}^2} \quad (12)$$

$$a_2 = -\frac{c_{m\alpha} * \mu + c_{L\alpha} * c_{mq}}{\bar{r_z}^2} \quad (13)$$

$$a_3 = \frac{-2 * c_L * [(c_L - c_{D\alpha}) * c_{mq} + c_L * c_{m\dot{\alpha}}]}{\bar{r_z}^2} \quad (14)$$

$$a_4 = \frac{-2 * {c_L}^2 * \mu c_{m\alpha}}{\bar{r_z}^2} \quad (15)$$

and

$$\bar{r_z}^2 = \frac{I_{yy}}{m * S^2} \quad (16)$$

$$\mu = \frac{2 * m}{\rho * S * C} \quad (17)$$

By solving equation (11), we obtain the eigen values of the system which indicate their natural frequencies and damping ratios.

In order to simplify the decomposition of the characteristic equation, Ostoslavsky supposed that the eigen values of the long mode is negligible with respect to the short mode, and finally the natural frequencies of the short and long modes can respectively obtained from:

$$\lambda^2 + \mathrm{a}_1\lambda + \mathrm{a}_2 = 0 \quad (18)$$

$$\lambda^2 + \frac{\mathrm{a}_2\mathrm{a}_3 - \mathrm{a}_1\mathrm{a}_4}{\mathrm{a}_2^2}\lambda + \frac{\mathrm{a}_4}{\mathrm{a}_2} = 0 \quad (19)$$

Another approach is used to identify the natural frequency in this case. It is well known from the definition of the eigen value

$$\lambda = \omega_n\zeta \pm \sqrt{(\omega_n\zeta)^2 - \omega_n^2} \quad (20)$$

the natural frequency can be calculated from the analysis of the left and right parts individually and comparing them with the formula of the roots of the second order equation.

4. Experiments

4.1 Experimental Setup

The experiments were conducted for the steady cruise flight of the airplane and the data were collected using three measuring devices, namely, ArduPilot [**Error! Reference source not found.**], SmartAP [[11]], and PixHawk [[10]]. To prevent miscellaneous disturbances, the airplane was controlled using “manual” mode without stability augmentation. During the flight the airplane was balanced so as it flies straight at constant velocity and altitude. Flight parameters were controlled form the ground station by means of telemetry link. The experiments were conducted at several days along the year to ensure repeatability and overcome miscellaneous factors. Besides, three sets of sensors were used independently for more accuracy and doubling the amount of data and also to stand on the difference between results for different sampling frequency, and different ways to measure flight angles. First set is the data obtained from the autopilot of type ArduPilot Mega which measure pitch, roll, and yaw angles of the aircraft and has sampling frequency of 3.7 Hz. The second dataset is obtained from PixHawk, which also uses the Eulerian representation of the angles, with sampling rate of 24 Hz.

The third dataset is from SmartAP that can measure with sampling frequency up to 250 Hz and use quaternions which provide a convenient mathematical notation for representing rotations and orientations of objects in three dimensions. It has some benefits compared to Euler angles as simplicity of composition and prevention of the gimbal lock problem. Besides, they are more numerically stable and efficient compared to rotation matrices [[13]].

To simulate the response of a big aircraft in case of small disturbance a mathematical model is created and its response is recorded in the form of flight path angles and compared to the oscillations from flight log of flight test. This method is not valid for UAVs because the flight velocity scale is close to the scale of disturbances, which can affect adversely the measured oscillations. In the current research, the flight data are measured then processed to find the most amplified frequencies in the Fourier domain.

4.2 Quaternions VS. Eulerian Representations for Rotation and Orientation

To convert quaternions to the conventional Eulerian representation, i.e. pitch, roll, and yaw, equation (21) can be used [[14]]. Sample of quaternions and their equivalent Euler angles are presented in figures 2 and 3 respectively.

$$\begin{bmatrix} \Phi \\ \theta \\ \psi \end{bmatrix} = \begin{bmatrix} \text{atan}\left(\frac{2(q_0*q_1+q_2*q_3)}{1-2(q_1^2+q_2^2)}\right) \\ \text{asin}\left(2(q_0*q_2-q_1*q_3)\right) \\ \text{atan}\left(\frac{2(q_0*q_3+q_1*q_2)}{1-2(q_2^2+q_3^2)}\right) \end{bmatrix} \tag{21}$$

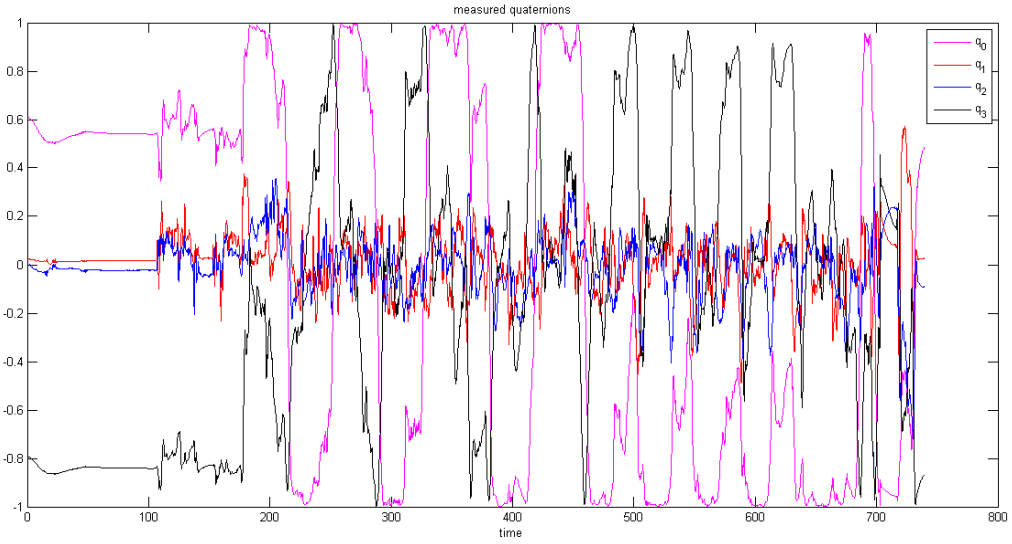

Figure 2 Quaternions measured during flight

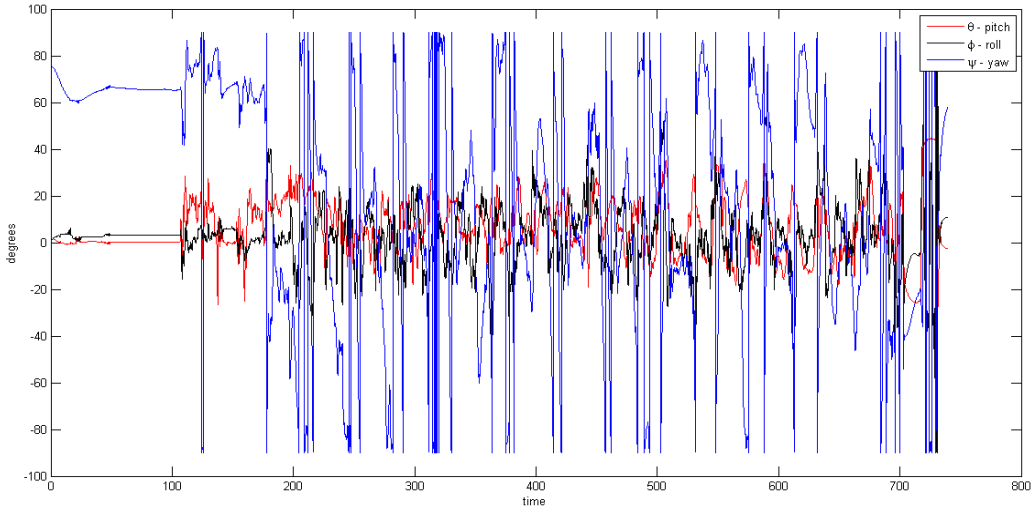

Figure 3 Euler angles calculated from quaternions.

Considering the devices used in the experimental measurement, the low-frequency device could not measure frequencies more than 2 Hz because of the sampling frequency restriction. The signal of the pitch angle from the ArduPilot and the transformed one from SmartAP are quite similar as shown in Figures 10 and 11 except in the peak points, as the high frequency device can capture it better. Samples shown in Figures 10 and 11 are for the same time period but shifted for better visualization. The blue line is for SmartAP and the red line represents the Ardupilot data.

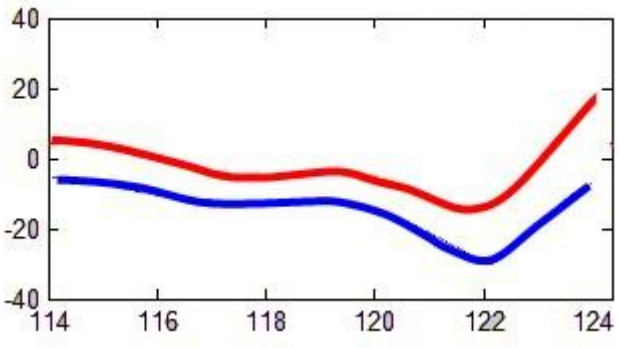

Figure 4 Sample 1 from SmartAP (blue) and ArduPilot (red) for the same time interval

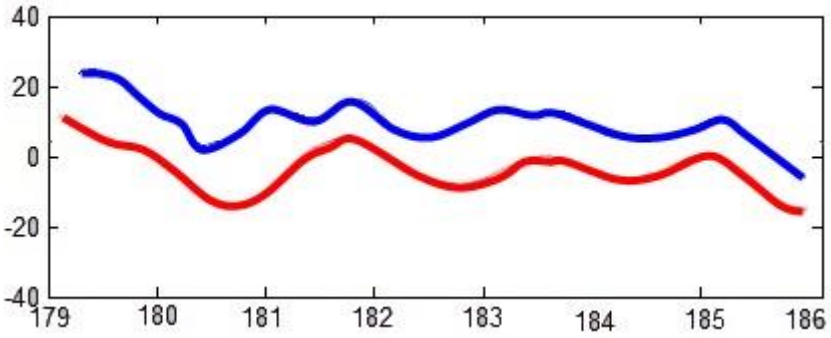

Figure 5 Sample 2 from SmartAP (blue) and ArduPilot (red) for the same time interval

4.3 Data Analysis

Due to the fact that the air disturbances are relatively high compared to the forces acting on the airplane, the ordinary method of validating the stability is not feasible for UAVs. Another method is introduced to surpass this issue through processing the flight angles and obtain the system main frequencies and compare them to the theoretical results [[7]]. Procedure of this method is as following: during the UAV flight the flight angles were recorded. After landing these data were retrieved and analysed by Fourier transform and the natural frequencies were obtained and compared to the ones calculated from the theoretical procedure.

To convert discrete time samples from time to frequency domain Fast Fourier Transform (FFT) is used. The data sets retrieved are processed by Fast Fourier Transform [[14]] with and without filtering. Sample of data signal of pitch angle is shown in Figure 6. While examining, it is taken into account the signal first and last points have the same values to avoid aliasing.

Data are filtered by Hanning filter to prevent leakage in the transform [**Error! Reference source not found.**]. Such filter is chosen for this case because:

1. The investigated signal is random with unknown frequency.
2. The vibrations are within narrow band.
3. The exact amplitude is not as important compared to the value of the frequency itself.
4. It overcome the noise and get the mean value of the frequency.

For these reasons, the most suitable filter is Hanning filter. Vibrations due to motor are not captured because its frequency is rather high and chaotic but it appears in terms of noise all over the signal. Figures 7 to 19 show samples of the obtained results at different periods of time.

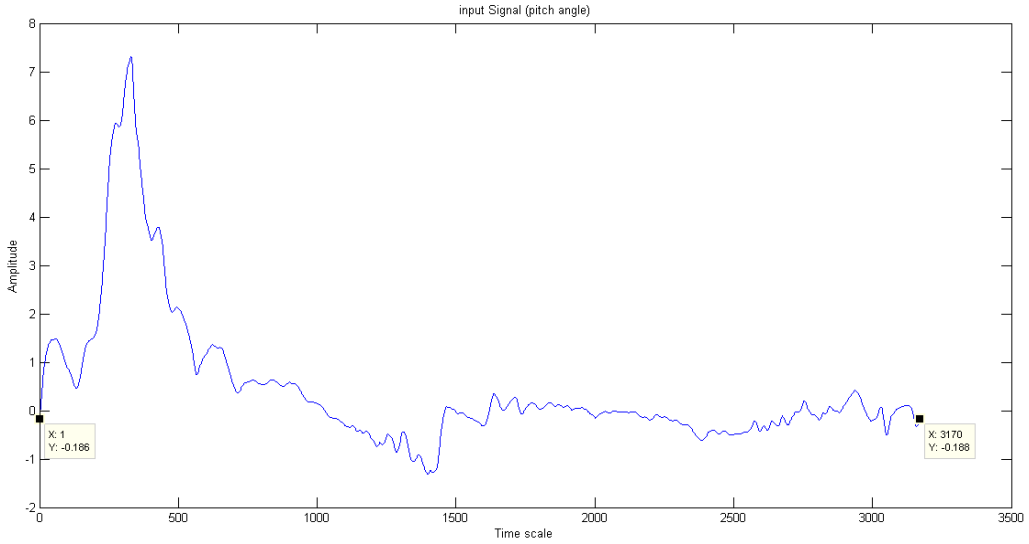

Figure 6 Sample for a signal which first and last points have the same values to prevent aliasing.

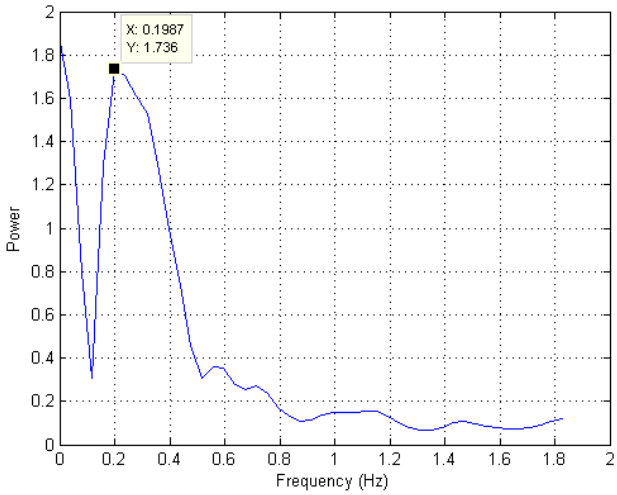

Figure 7 Sample of long mode frequency for Sonic 185 (ArduPilot)

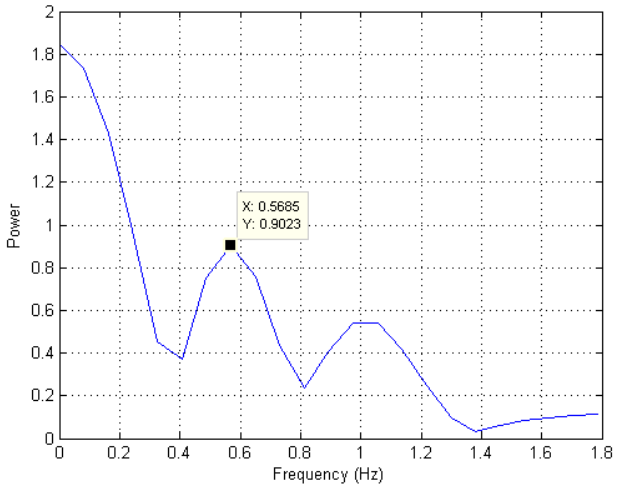

Figure 8 Sample of dutch roll frequency for Cirrus (ArduPilot)

The data samples are collected at different speeds with different devices as shown in Figures 8 to 19. After the analysis the experimentally-obtained natural frequencies are compared to the ones calculated form the theoretical approach. The results show good agreement as illustrated in Tables 8 and 9. Tolerance of the experimental results varies from ± 0.04 to ±0.1 Hz in the most critical cases.

Table 8 Short mode frequencies of Sonic 185 at different flight speeds, in Hz

velocity	experiment	Calculation (Roskam)	Device
6.5	0.7	0.72	ArduPilot
7	1.0	0.79	pixhawk
8	1.2	0.96	SmartAP
9	1.1	1.05	ArduPilot
10	1.2	1.14	pixhawk
12	1.4	1.36	pixhawk

Table 9 Long mode frequencies of Sonic 185 at different flight speeds, in Hz

velocity	experiment	Calculation (Roskam)	Device
10	0.187	0.1874	pixhawk
12	0.191	0.1909	pixhawk

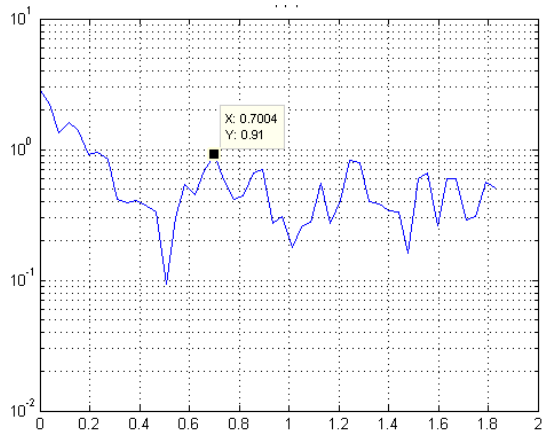

Figure 9 Measured frequency at velocity = 6.5 m/s, from ArduPilot.

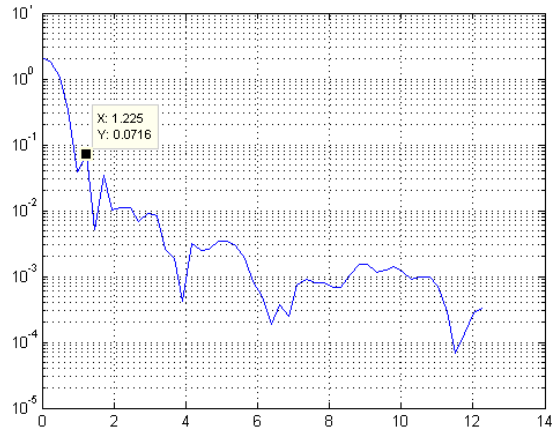

Figure 10 Measured frequency at velocity = 10 m/s, from PixHawk

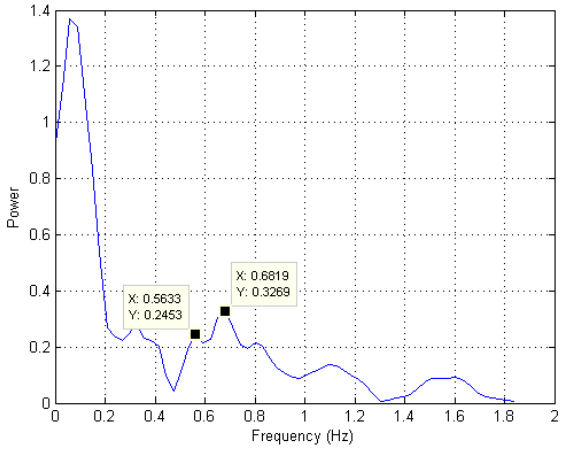

Figure 11 Sample of Dutch roll mode from ArduPilot

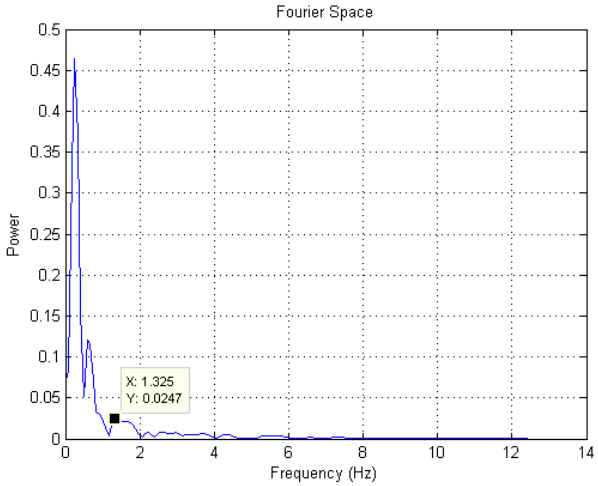

Figure 12 Sample of short mode from PixHawk

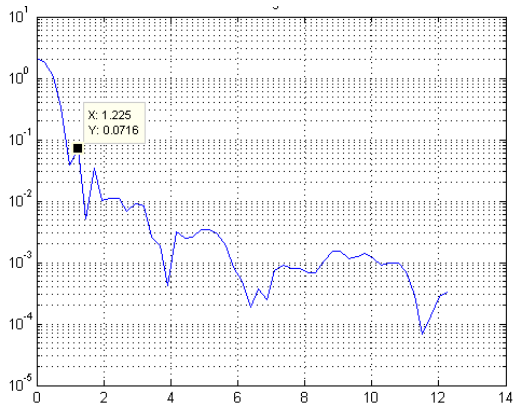

Figure 13 Sample of short mode from PixHawk

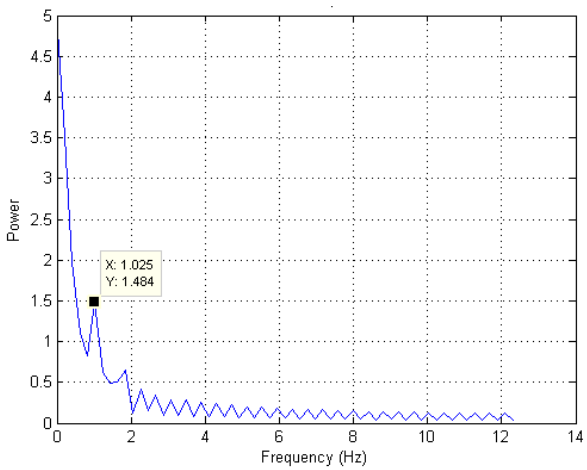

Figure 14 Sample of short mode from PixHawk.

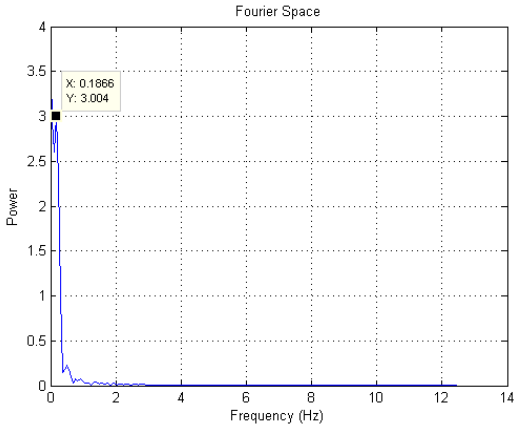

Figure 15 Measured frequency at velocity of 7 m/s, sampling rate – 12 Hz from PixHawk.

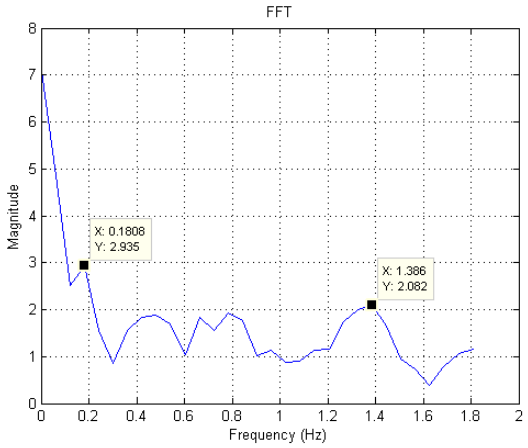

Figure 16 Sample of long and short modes frequency

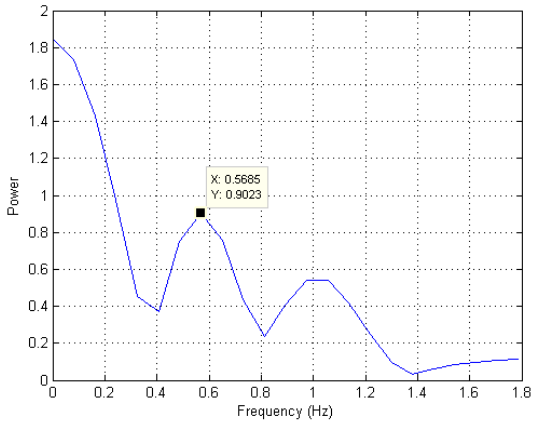

Figure 17 Sample of dutch roll frequency for Cirrus (ArduPilot)

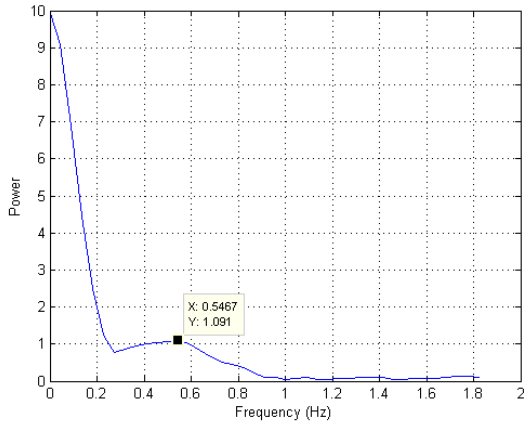

Figure 18 Sample of dutch roll frequency for Cirrus (SmartAP)

5. Conclusion

Due to the differences in the aerodynamic and geometrical scales between large and small / mini UAVs, the stability characteristics may differ. Hence, this paper studies the disturbed motion natural frequencies of small Unmanned Aerial Vehicles (UAVs) of glider type and evaluate the available analytical methods based on extended experimental results obtained from different measuring devices and at different velocities for two aircraft.

It is found that the experiments and exact analytical method of Roskam are well matched over the investigated range. Using low-sampling-rate device in measuring the flight path angles is acceptable under the condition that its frequency is higher than the short mode frequency. The presented method of flight data analysis is independent of the orientation/rotation representation system used in the gyroscope measuring devices.

6. Copyright Statement

References

[1] Roskam, J. (1995). Airplane flight dynamics and automatic flight controls. DAR Corporation.

[2] Hull, D. G. (2007). Fundamentals of airplane flight mechanics. Springer.

[3] Ostoslavsky, I. V. (1957). Aerodynamics of Aircraft. Oborongiz, Moscow.

[4] M. El-Salamony, S. Serokhvostov, A. Epikhin, and K. Zaripov, 2016. Comparison between experimental, analytical, and numerical methods in natural frequencies of the longitudinal flight modes for small UAVs. In Proc of International Micro Air Vehicle Conference (IMAV 2016), Beijing, China.

[5] M. El-Salamony, S. Serokhvostov, A. Epikhin, and K. Zaripov, 2016. Measurement and calculation of natural frequencies of the longitudinal flight modes for small UAVs. In Proc of Extremal and Record-Breaking Aircrafts Workshop (ERBA 2016), Zhukovsky, Russia.

[6] M. El-Salamony, S. Serokhvostov, 2017. Validation of Natural Frequencies Formulas of Flight Modes for Small UAV. In Proc of European Conference for Aeronautics and Aerospace Sciences (EUCASS 2017), Milan, Italy.

[7] M. El-Salamony, S. Serokhvostov, 2018. Fuselage Effect on Small UAVs Natural Frequencies. In Proc of Extremal and Record-Breaking Aircrafts Workshop (ERBA 2018), Zhukovsky, Russia.

[8] Universal Power Enterprizes Ltd. (2008). Sonic 185: Instruction manual. Universal Power Enterprizes Ltd., Kowloon, Hong Kong, 2008.

[9] Reichard Modelsport, 2008. Cirrus Instruction manual.

[10] Coombes, M., McAree, O., Chen, W. H., & Render, P. (2012, September). Development of an autopilot system for rapid prototyping of high level control algorithms. In Proceedings of 2012 UKACC International Conference on Control (pp. 292-297). IEEE.

[11] Shilov, K. 2014. The next generation design of autonomous MAV flight control system SMARTAP. In IMAV 2014: International Micro Air Vehicle Conference and Competition 2014, Delft, The Netherlands, August 12-15, 2014. Delft University of Technology.

[12] Meier, L., Tanskanen, P., Fraundorfer, F., & Pollefeys, M. (2011, May). Pixhawk: A system for autonomous flight using onboard computer vision. In 2011 IEEE International Conference on Robotics and Automation (pp. 2992-2997). IEEE.

[13] Hamilton, W. R. (1844). Ii. on quaternions; or on a new system of imaginaries in algebra. The London, Edinburgh, and Dublin Philosophical Magazine and Journal of Science, 25(163), 10-13.

[14] Diebel, J. (2006). Representing attitude: Euler angles, unit quaternions, and rotation vectors. Matrix, 58(15-16), 1-35.

[15] Heckbert, P. (1995). Fourier transforms and the fast fourier transform (fft) algorithm. Computer Graphics, 2, 15-463.

[16] Madisetti, V. (Ed.). (1997). The digital signal processing handbook. CRC press.